Biosensors and Bioelectronics 196 (2022) 113697

Contents lists available at ScienceDirect

Biosensors and Bioelectronics

journal homepage: www.elsevier.com/locate/bios

Nanoparticle-assisted detection of nucleic acids in a polymeric nanopore with a large pore size

Youwen Zhang [a], Xiaohan Chen [a], Ceming Wang [b], Hsueh-Chia Chang [b], Xiyun Guan [a,*]

[a] Department of Chemistry, Illinois Institute of Technology, 3101 S Dearborn St, Chicago, IL, 60616, USA
[b] Department of Chemical and Biomolecular Engineering, University of Notre Dame, Notre Dame, IN, 46556, USA

ARTICLE INFO

Keywords:
Solid-state nanopore
PET film
DNA
Biomarker
Viral RNA

ABSTRACT

Rapid and accurate detection of nucleic acids is of paramount importance in many fields, including medical diagnosis, gene therapy and virus identification. In this work, by taking advantage of two DNA hybridization probes, one of which was immobilized on the surface of gold nanoparticles, while the other was free in solution, detection of short length nucleic acids was successfully achieved using a large size (20 nm tip diameter) polyethylene terephthalate (PET) nanopore. The sensor was sensitive and selective: DNA samples with concentrations at as low as 0.5 nM could be detected within minutes and the number of mismatches can be discerned from the translocation frequency. Furthermore, the nanopore can be repeatedly used many times. Our developed large-size nanopore sensing platform offers the potential for fieldable/point-of-care diagnostic applications.

1. Introduction

The capability of rapid and accurate detection of specific target gene sequences and their base variations provides many opportunities in modern medicine. Such a diagnostic technology not only benefits early disease detection, but also enables personalized treatment to improve outcomes. Furthermore, the recent rapid spread of novel coronavirus disease (COVID-19) pandemic has reinforced the importance of needing a prompt and accurate nucleic acid analysis technology that is easily deployable and manufacturable (Arima et al., 2021). The current gold standard for gene detection is PCR. Although accurate, its expensive optical detectors render it unsuitable for many applications (Feng et al., 2020; Tellinghuisen and Spiess, 2014; VanGuilder et al., 2008). More recently, the development of next-generation DNA sequencing technologies makes it possible to rapidly read long sequences of DNA samples. However, these long read sequencers suffer from relatively high error rates although this drawback can be improved by the significant advancement in bioinformatics for base-calling and error correction (Kono and Arakawa, 2019). Another popular strategy to detect nucleic acids, especially biomarkers, is the use of DNA hybridization, where a complementary DNA or PNA probe is employed to detect whether or not there is presence of a short target nucleic acid sequence in a sample (Mereuta et al., 2020). Various sensitive nano-biotechnologies, including fluorescence, colorimetric, electrochemistry, resonance, and FET-based biosensors have been reported (Chaibun et al., 2021; Jiao et al., 2020; Liang et al., 2020; Wu et al., 2020; Zhao et al., 2020). However, most of these methods require the use of labels or expensive instruments.

By monitoring the ionic current modulations produced by the interaction between analyte molecules and a nanoscale-sized channel (Chen et al., 2018a; Roozbahani et al., 2020; Wang et al., 2021b), nanopore stochastic sensing, a label-free technology, has successfully been utilized to explore various applications, including DNA sequencing (Bayley, 2017; Branton et al., 2008), biosensing (Chen et al., 2019; Roozbahani et al., 2019) and environmental monitoring (Roozbahani et al. 2017, 2018) at the single-molecule level. At present, there are two major types of nanopore technology: biological protein pore and synthetic solid-state nanopore (Zhang et al., 2020a). The former generally provides a better resolution and selectivity to analyte detection than the latter. However, the practical application of the protein pores was limited by the fragile lipid bilayer used for supporting the sensing element. In contrast, solid-state nanopores are stable and could tolerate a variety of extreme conditions, and offer the potential for large-scale integration with on-chip electronics, which are ideal for field deployable applications and can provide higher throughput than protein nanopores (Goto et al., 2018; Haque et al., 2013). However, two major hurdles need to be overcome before solid-state nanopores could be used as a versatile tool for various applications. First, the currently available

* Corresponding author.
E-mail address: xguan5@iit.edu (X. Guan).

https://doi.org/10.1016/j.bios.2021.113697
Received 22 August 2021; Received in revised form 3 October 2021; Accepted 7 October 2021
Available online 8 October 2021

synthetic nanopore sensor has a large background noise and a poor sensitivity/resolution. Second, the size and the shape of the synthetic nanopore is difficult to be reproduced with desired precision, so that variations occur from pore to pore and from batch to batch (Haque et al., 2013). On the other hand, compared with small size (sub-10 nm) synthetic nanopores, nanopores with large pore sizes (e.g. 10–20 nm) are much easier to fabricate and are commercially available (Xia et al., 2018). They can also be readily etched into reproducible conic or other shape geometries to enhance the sensitivity (Wang et al., 2021a). However, the nanopore performance generally decreases with an increase in the pore diameter. To be more specific, in terms of detecting dsDNA or ssDNA with a complementary probe, 22-mer nucleic acids could be detected at concentrations as low as 0.1 pM by a protein pore with a constriction of ~1.5 nm (Wang et al., 2011). In contrast, small diameter synthetic nanopore such as a 3.6-nm diameter HfO_2 pore was only able to detect 100-bp dsDNA at nanomolar concentrations (Larkin et al., 2013), while large diameter (>10 nm) solid-state nanopores were usually used to investigate dsDNA of several to dozens of kbps (Kumar Sharma et al., 2019; Wang et al., 2018b). Unlike the various efforts in the recent years toward developing functionalized synthetic nanopores to improve sensor sensitivity (Wang et al., 2021a; Zhang et al., 2020a), herein, we report a new strategy to overcome the low resolution of the large-size solid-state nanopores by taking advantage of gold nanoparticles (AuNPs) and multiple DNA hybridization probes for rapid and sensitive detection of nucleic acids.

2. Experimental section

2.1. Materials and reagents

Citrate-capped AuNPs with 3-nm diameter were purchased from Nanopartz Inc. (Loveland, CO). All the DNA molecules were obtained from Integrated Technologies (IDT, Coralville, IA). These include 5′–$(CH_2)_6$–S–S-$(CH_2)_6$-AAAAAA-ATGGACCCCAAAATC-3′ (P1), 5′-AGCGAAATGCACCCC-AAAAAA–$(CH_2)_3$–S–S–$(CH_2)_3$–3′ (P2), 5′-GGGGTGCATTTCGCT-GATTTTGGGGTCCAT-3′ (Target ssDNA), and a series of mutant DNA samples which differ from the target DNA by one mismatch, two mismatches, three mismatches, four mismatches, and other multiple mismatches (Table S1). Note that the target nucleic acid is a 30-mer ssDNA fragment from the sequence of SARS-CoV-2 (Chu et al., 2020). All the other chemicals, including Tris(2-carboxyethyl) phosphine hydrochloride (TCEP), potassium chloride, Trizma base, hydrochloric acid, HPLC-grade water, and DNase- and RNase-free water, were purchased from Sigma-Aldrich (St. Louis, MO). The stock solutions of all DNA samples were prepared in nuclease-free water at a concentration of 1 mM each and stored at −20 °C before and immediately after use. The reaction buffer for nucleic acid hybridization contained 10 mM Tris, 1 mM EDTA, 100 mM NaCl, and 2 mM $MgCl_2$ (using HCl to adjust the pH of the solution to pH 8.0). The nanopore sensing buffer was consisted of 10 mM Tris, 1 mM EDTA, and 500 mM KCl (using HCl to adjust the pH of the solution to pH 8.0).

Preparation of ssDNA-conjugated AuNP probe. For preparation of ssDNA-conjugated AuNP probe (AuNP-P1), 25 μL of disulfide-terminated oligonucleotide (P1, 1 mM) was first reacted with 250 μL of TCEP (10 mM) for 1 h at room temperature to reduce the disulfide bond and yield thiol-terminated DNA (Li et al., 2013). The thiol-terminated DNA was then mixed with 250 μL of 3.0 nm-diameter AuNP solution (39.2 μM). After incubation at room temperature for 16 h, the mixture was slowly added to 50 μL of NaCl solution (4 M), followed by sonication for 10 s. Since both ssDNA and AuNPs are negatively charged, a high concentration of salt is needed to screen the long-ranged charge repulsion to enable DNA adsorption on the surface of AuNPs (Zhang et al., 2012a). Then, the solution was centrifuged at 13,500 rpm for 10 min to separate the AuNP-P1 from the unreacted reagents. The product (AuNP-P1) was then washed with 50 μL of PBS buffer (10 mM Na_2HPO_4, pH 8.0) containing 0.01% Tween20, and redispersed in HPLC-grade water. Long-term storage could be carried out at relatively low temperature (4 °C) for several months in low salt and slightly acidic condition (Bhatt et al., 2011; Epanchintseva et al., 2019; Li et al., 2013).

DNA Hybridization. Briefly, 10 μL of AuNP-P1 (200 μM) and 2 μL of target ssDNA (1 mM) were mixed with a 28-μL Tris reaction buffer solution, and incubated at 65 °C for 10 min, followed by cooling to room temperature. Then, an extra 2 μL of P2 DNA probe (1 mM) was added to the above mixture, and incubated at 40 °C for 20 min, followed by cooling to room temperature.

Fabrication of the conical shaped polymeric nanopore. Details on the fabrication of single asymmetric nanopores in polyethylene terephthalate (PET) membrane have been described in our previous work (Zhang et al., 2020a). Briefly, the 12-μm thick polyethylene terephthalate (PET) foils were irradiated with single swift heavy ions (Au) with energy of 11.4 MeV per nucleon at the GSI in Darmstadt, German and then subsequently etched at room temperature (295 K) by an asymmetric etching method, where the foil was mounted between two isolated containers that contained an etchant solution of 2.5 M NaOH in 1:1 MeOH/H_2O and a stopping solution of 1 M HCOOH and 1 M KCl, respectively. A secondary symmetric etching process (2 M NaOH) was applied to enlarge the tip size. In all cases, the diameter of the base was around 1000 ± 80 nm, as determined by electron microscopy (Fig. S1). The final tip diameter was ~19.7 nm, which was calculated by the following equation: $d_{tip} = 4IL/\pi\kappa DV$, where I/V is the slope of the current-versus-voltage in 1 M KCl solution and was calculated from the produced ionic current at an applied voltage bias ranging from −100 mV to +100 mV (Fig. S1). D is the base diameter (D = 1 μm), and κ is the special conductivity of the electrolyte. For 1 M KCl solution at 25 °C, κ is 0.11173 $\Omega^{-1}cm^{-1}$. L is the length of the channel, which is approximated to the thickness of the membrane after chemical etching (11.5 μm).

Electrochemical recording. Unless otherwise noted, all the analyte species, including AuNP-P1 and its hybridization products were added to the nanopore base compartment. Currents were recorded with a patch clamp amplifier (Axopatch 200B, Molecular Devices; Sunnyvale, CA, USA). Data analysis was carried out using pClamp 10.7 (Molecular Devices). Each single-channel current trace was recorded for at least 5 min. The detailed procedure for patch clamp experiments, including instrument parameters and data analysis, has been provided in our previous work (Chen et al. 2018a, 2018b). All the experiments were performed in a 2.0 mL nanopore sensing buffer solution at 26 ± 1 °C with an applied voltage bias (via a pair of Ag/AgCl electrodes) ranging from −1 V to 1 V. Both symmetric (with both the base and tip compartments filled with 0.5 M KCl buffer solution) and asymmetric (with the base compartment filled with 0.5 M KCl, whereas the tip compartment filled with 1–2 M KCl) electrolyte conditions were investigated in this study.

Instrument. The UV–vis absorption spectra of AuNPs, AuNP-P1 and ssDNA P1 were obtained using a DU 800 UV–VIS spectrophotometer (Beckman Coulter, Fullerton, CA). The size distribution of AuNPs and their complexes was recorded using dynamic light scattering (Zetasizer Nano S, Malvern Instruments Ltd, Worcestershire, UK).

3. Results and discussion

3.1. Principle of our developed nucleic acid detection strategy using a solid-state nanopore having a large pore size

Compared with a small diameter nanopore, using a solid state nanopore having a large pore size as the stochastic sensing element has advantages of easier production and improved reproducibility. However, the poor sensor sensitivity/resolution (due to low comparability between the size of the analyte and the diameter of the nanopore and the high translocation velocity of the analyte for event picking up limits its practical application (Roman et al., 2017; Vlassiouk and Siwy, 2007). Unlike the various efforts in the recent years, including ours, toward developing functionalized synthetic nanopores to improve sensor sensitivity (Li et al., 2019; Wang et al., 2021a; Zhang et al., 2020a), in

this work, we take advantage of AuNPs and multiple ssDNA hybridization probes to overcome the low resolution of the solid-state nanopores with large pore diameters, thus achieving rapid and highly sensitive detection of nucleic acids. The AuNP allows capture of multiple targets to increase the size and charge of each NP complex. Earlier theoretical work shows that when the complex size approaches the pore size and when the complex charge is sufficiently high, intrapore concentration polarization can occur to amplify the signal amplitude more than just the area ratio due to the excluded volume current blockage effect (Sensale et al., 2020). Our earlier work also shows that, due to its shorter persistence length, ssDNAs produce longer translocation time than dsDNAs (Wang et al., 2021a). We hence utilize long DNA probes with unpaired end sequences and sandwich complexes with two end probes. The sandwich complex offers another advantage—selectivity. In our earlier work, we developed a nanofluidic platform based on depletion isotachophoresis in agarose gel generated by an ion-selective membrane to improve the selectivity of DNA detection. We found that the high electric field in the nanofluidic channel could break up AuNPs sandwich structures with only 2 mismatches (Marczak et al., 2017).

As shown in Scheme 1, AuNPs and/or short ssDNA would not cause current modulation events in a large diameter nanopore. In contrast, after thiol-terminated ssDNA is attached to the surface of AuNPs, short duration and small amplitude current modulation events could be observed when the produced AuNPs-ssDNA conjugate (AuNP-P1) passes through the nanopore due to its larger molecular size than free AuNPs and ssDNA. If the sample solution contains the target nucleic acid (DNA or RNA), the hybridization product (AuNP-P1-NA) between the target nucleic acid and AuNP-P1 would produce a new type of events with larger blockage amplitude and/or residence time than those of AuNP-P1. To further improve the resolution and performance of the nanopore, a second ssDNA hybridization probe (P2), which is complementary to another portion of the target DNA, is added. The resultant AuNPs/nucleic acid conjugate (AuNP-P1-NA-P2) would induce another type of events with significantly different signatures from those of AuNP-P1-NA due to the change in molecular geometry and structure. Taken together, the combined AuNP-P1-NA and AuNP-P1-NA-P2 event signatures would allow accurate detection of the target nucleic acid. For proof-of-concept demonstration of this new strategy, an unmodified PET nanopore (base diameter: ~1000 nm; tip diameter: ~20 nm) was used as the sensing element, while a 30-mer ssDNA fragment (from the sequence of SARS-CoV-2 (Chu et al., 2020)) was chosen as the target nucleic acid. Both the DNA probes P1 and P2 contain a core fragment of 15 bases (which is complementary to the 30-mer target nucleic acid) and an additional spacer of 6-adenine bases (for facilitating the hybridization between DNA probes and the target nucleic acid (Demers et al., 2000)). It should be noted that, the length of the probe DNA is critical to its efficient attachment to the surface of AuNPs. In general, the longer the DNA probe is, the fewer DNA molecules can be absorbed on AuNPs (Lu et al., 2015; Steel et al., 2000). Furthermore, it was reported that the adsorption of short ssDNA on AuNPs was much faster than that for long DNA (Zhang et al., 2012b). In addition, when DNA strands were less than ~30 bases long, shorter than its persistence length, the sizes of the produced Au/DNA conjugates were around the sum of the AuNPs diameter plus twice the length of the fully stretched single-stranded DNA due to the fully stretched and densely packed structure (Parak et al., 2003). Therefore, using relatively short DNA probes benefits the diameter control of the resultant AuNPs/nucleic acid conjugate.

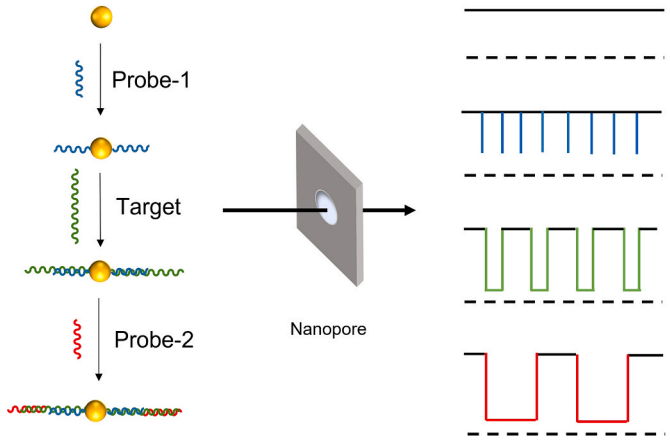

Scheme 1. The principle of nucleic acid detection using a large pore size solid-state nanopore.

3.2. Characterization of AuNP-P1 and its nucleic acid hybridization products

The successful attachment of DNA probe P1 to the surface of AuNPs was supported by UV–vis absorption spectroscopy. As shown in Fig. S2a, the AuNPs (0.1 μM) sample had a band at around 512 nm due to the surface plasmon resonance (SPR) of spherical gold nanoparticles. In contrast, an absorption peak at ~530 nm was observed for the AuNP-P1 (0.1 μM) solution. The red-shift (~18 nm) was due to the partial surface encapsulation of AuNPs by DNA, which weakened the optical properties of AuNPs (He et al., 2018). Furthermore, the AuNP-P1 sample had a large absorbance peak at 260 nm. This peak was similar to that (263 nm) of bare P1 but was not observed in the AuNPs solution. The density of the ssDNA probes on the 3-nm AuNPs surface was estimated using a colorimetric-based assay (Kim et al., 2019; Zhang et al., 2020b). The valency of 3-nm AuNPs was 2.7 ssDNA, which was close to that (2–6) of AuNPs with similar sizes reported by other groups (Ohta et al., 2016). In addition, DLS analysis provided further evidence for the successful conjugation between P1 and AuNPs. As shown in Fig. S2b, the free AuNPs solution showed a peak at 4.0 ± 1.0 nm, while a new peak at 17.0 ± 7.0 nm was identified for the AuNP-P1 sample. After addition of the target DNA to the AuNP-P1 solution, another peak at 22 ± 6.0 nm was observed, demonstrating the formation of AuNP-P1-NA hybridization complex. It should be noted that, the more DNA molecules attached on the AuNP surface, the less non-specific adsorption between AuNPs and nucleic acids would occur (Chen et al., 2016), which was supported by the narrower band of AuNP-P1-NA than that of AuNP-P1.

3.3. Nanopore detection of target nucleic acids

For proof-of-concept demonstration of the feasibility of utilizing a large size nanopore as a single-molecule stochastic sensing element for detection of nucleic acids, translocation of AuNP-P1 and its hybridization complexes in the nanopore was initially investigated at an applied potential bias of +800 mV in an electrolyte buffer solution containing a 0.5 M KCl, 10 mM Trizma base and 1 mM EDTA (pH 8.0). As controls, the interactions between AuNPs/nucleic acids (P1, P2 and NA) and the nanopore were also studied under the same experimental conditions. As we expected, AuNPs, P1, P2 and NA rarely produced any observable current modulation events in the nanopore because of their incompatible sizes and rapid translocation velocity (note that the diameters of AuNPs and ssDNA are ~3 nm, and ~1.4 nm, respectively, while the nanopore had a tip diameter of ~20 nm). In contrast, the ssDNA immobilized AuNPs (AuNP-P1) showed frequent current modulations with a mean blockage amplitude of 53 ± 5 pA and a mean residence time of 0.24 ± 0.08 ms (Fig. 1 and S3). After hybridization with the target ssDNA, the AuNP-P1-NA complex produced a new type of events (blockage amplitude: 110 ± 10 pA; residence time: 2.1 ± 0.4 ms, Fig. 1 and S4). The larger blockage amplitude and longer residence time of these new events than those of free AuNP-P1 are beyond the increase in the excluded volume for ion current (Oukhaled et al., 2011; Talaga and Li, 2009) and suggests intropore ionic strength polarization is important (Sensale et al., 2020). Similar to the hybridization between AuNP-P1 and NA, addition of the second DNA probe P2 to the AuNP-P1-NA

solution produced another event with quantitatively deconvoluted translocation signatures (blockage amplitude: 150 ± 8 pA; residence time: 2.4 ± 0.3 ms) in the nanopore. To be more specific, under our experimental condition, the mixture sample showed three distinct types of events (blockage amplitude: 53 pA, 110 pA, and 150 pA), which were corresponding to the free AuNP-P1, free AuNP-P1-NA, and AuNP-P1-NA-P2 complex, respectively (Fig. 1 and S5).

3.4. Effect of applied voltage bias and probe ratio on nanopore performance

Previous studies including ours have shown that the potential applied across the nanopore played an important role in the resolution/performance of the nanopore sensor (Chen et al., 2019; Zhang et al., 2020a). In order to find an appropriate potential bias for sensitive detection of nucleic acids, translocation of AuNP-P1 and its hybridization complexes in the large size nanopore was investigated at a series of voltages ranging from +400 mV to +1000 mV. Our experimental results (Fig. 2) showed that, as the applied potential bias increased, both the frequency and the blockage amplitude of the AuNP-P1, AuNP-P1-NA and AuNP-P1-NA-P2 events increased, while their event residence time decreased. In particular, the blockage amplitudes of the three species were significantly different at low voltages, so that AuNP-P1, AuNP-P1-NA and AuNP-P1-NA-P2 could be well separated. However, their distinction became less clear at a higher voltage. In terms of the event residence time, AuNP-P1 was well distinguishable from AuNP-P1-NA and AuNP-P1-NA-P2 at all the applied potentials, but the latter two species had similar values, which might be attributed to their similar radium to charge ratios (note that $\tau = 6\pi\eta rL/zeE$, where τ is translocation time, z is the charge, e is the electronic charge, E is the electric field strength, η is the solution viscosity, r is the radius of the molecule and L is the length of the pore) (Harrell et al., 2006). On the other hand, we found that the AuNP-P1 events were much more frequent than those of AuNP-P1-NA and AuNP-P1-NA-P2, which is not unreasonable considering that AuNP-P1 contained single-stranded DNA species, while double stranded DNA molecules were coupled to the surfaces of AuNP-P1-NA and AuNP-P1-NA-P2. Since all the three event parameters (amplitude, residence time, and frequency) had relatively large values at +600 mV, this voltage bias was chosen as the optimum applied potential, and used in the remaining experiments.

To further improve nanopore sensor sensitivity, the effect of the concentration ratio of P2 to AuNP-P1 on nanopore detection of nucleic acids was examined. We found that, with an increase in the concentration ratio, the frequency of the AuNP-P1-NA-P2 events increased significantly until the ratio reached 2.0 : 1.0, after which it began to saturate (Fig. 3), while that of the AuNP-P1-NA events decreased. The ratio of 2.0 : 1.0 was chosen as the optimum concentration ratio of P2 to AuNP-P1 and used in the remaining experiments, since under this experimental condition, the event frequency of AuNP-P1-NA-P2 was relatively high, while the amount of P2 consumed was relatively small.

3.5. Sensor sensitivity and selectivity

To determine the sensitivity of our developed large size nanopore sensing strategy, the interaction between AuNP-P1 and the 20-nm tip diameter PET nanopore was studied under the optimized experimental conditions (i.e., +600 mV, having the concentration ratio of P2 to AuNP-P1 of 2:1) in the presence of the target ssDNA with varying concentrations ranging from 25 nM to 200 nM and without/with P2. As shown in Fig. 4, the frequency of both the AuNP-P1-NA and AuNP-P1-NA-P2 events increased linearly with an increase in the analyte concentration. The corresponding correlation relationships have the form of $y = 0.0312x + 0.0742$ ($R^2 = 0.9361$) and $y = 0.07825x + 0.0926$ ($R^2 = 0.9722$), respectively. The limit of detection (LOD) of the nanopore sensor based on AuNP-P1-NA-P2 events was ~9.7 nM, where LOD was defined as the concentration of target nucleic acid corresponding to the signal of the blank plus three times its standard deviation (Armbruster and Pry, 2008). It should be noted that smaller nanopores (8 nm diameter) with Alumina surface modification was able to reach pM or even fM LOD for DNA targets of the same length (Wang et al., 2021a). The alumina insulation allows deeper field penetration into the bulk fluid and hence higher translocation event frequency. We hence believe

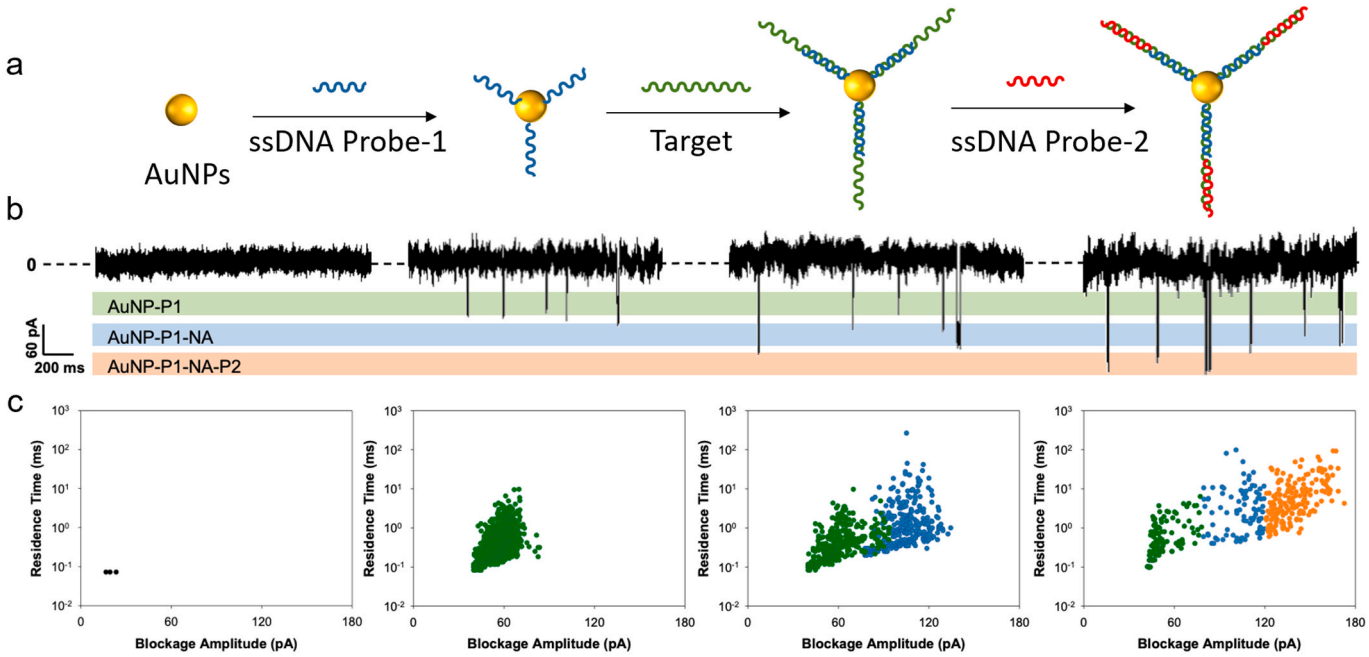

Fig. 1. (a) Schematic illustration of the method and procedure of detecting target ssDNA in a large-size solid-state nanopore; (b) typical trace segments of different species; and (c) their corresponding scatter plots of event residence time vs current blockage amplitude. The experiments were performed at +800 mV using a 20-nm diameter PET nanopore in a symmetric buffer condition with both the base and tip compartments filled with 0.5 M KCl and 10 mM Tris (pH 8.0). Uninterrupted 2-min single-channel recording traces were displayed in Figures S3-5.

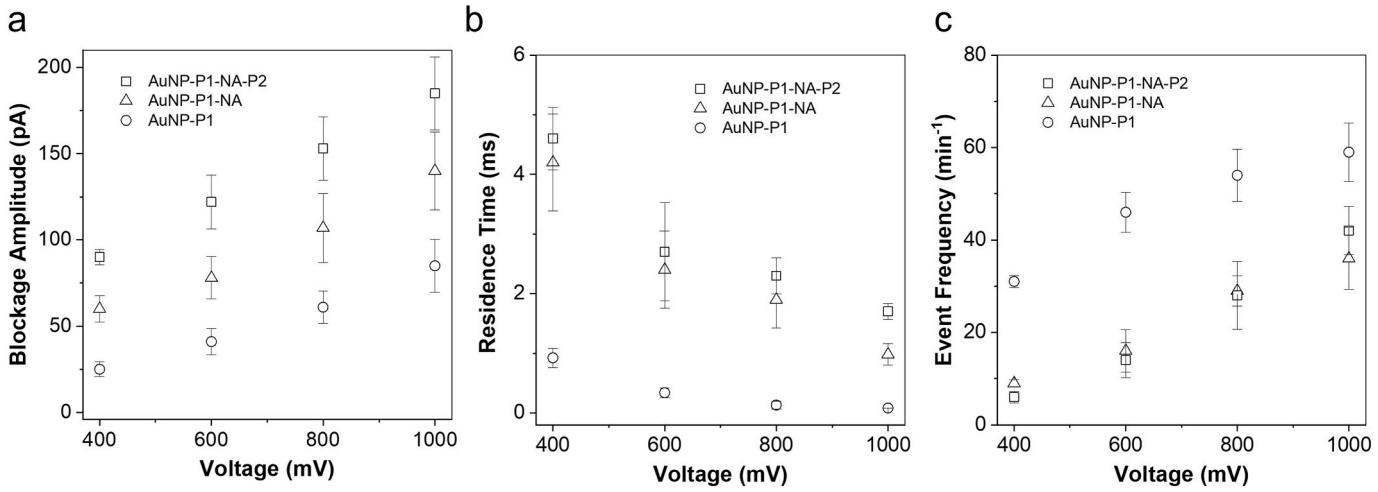

Fig. 2. Voltage effect on the characteristics of the current modulation events. (a) Blockage amplitude; (b) residence time; and (c) event frequency. The experiments were performed using a 20-nm tip diameter PET nanopore in a symmetric buffer condition with both the base and tip compartments filled with 0.5 M KCl and 10 mM Tris (pH 8.0). The concentrations of AuNP-P1, target ssDNA, and P2 were 1 μM each.

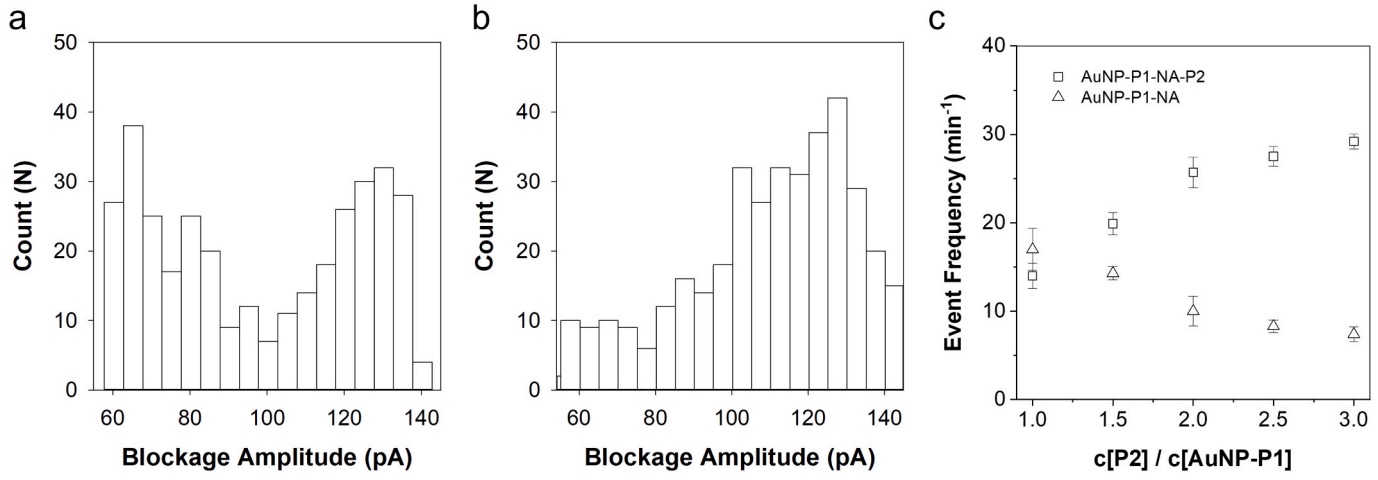

Fig. 3. Effect of the ratio of P2 concentration to AuNP-P1 concentration on the event distribution of the hybridization products. Representative event amplitude histograms of (a) 1:1 ratio and (b) 2: 1 ratio; and (c) plot of event frequency versus the ratio of P2 concentration to AuNP-P1 concentration. The experiments were performed at +600 mV in a symmetric buffer condition with both the PET nanopore base and tip compartments filled with 0.5 M KCl and 10 mM Tris (pH 8.0).

that orders of magnitude improvement of the LOD is possible. However, nM sensitivity is sufficient for detection of PCR amplicons.

To examine the selectivity of our developed multiple-probes nanopore sensing strategy, a series of mutant DNA samples which differ from the target DNA by one mismatch, two mismatches, three mismatches, four mismatches, and multiple (>5) mismatches (see Table S1 for their sequences) was examined. We found that, with the exception of the samples which had multiple (>5) mismatches from the target DNA, all the other mismatch samples produced current modulations in the PET nanopore. Similar to the full-match DNA, the events of these mismatch samples could also be categorized into two classes, which were attributed to AuNP-P1 and AuNP-P1-P2 hybridization products, respectively. Unfortunately, since these events had similar blockage amplitude and residence time values to those of the full-match target DNA, it is difficult to differentiate mismatch DNA samples from the complete-match sample based on these two parameters, indicating the low resolution of the large size unmodified PET nanopore. On the other hand, we noticed that, with the exception of the one-mismatch DNA, all the other mismatch DNA samples had significantly smaller number of events than the complete-match DNA (Fig. 5a), indicating the two base-mismatch resolution of the nanopore sensor. Our experimental data also suggested that mismatched DNA formed less stable hybridization products with AuNP-P1 and/or AuNP-P1-P2 than the full-matched DNA did, so that many of their translocation events could not be captured by the low resolution PET nanopore sensor (Dorris et al., 2003; Machinek et al., 2014). This is consistent with our earlier work that the sandwich complex with two or more mismatches can be broken up by the high field in the nanopore such that the number of detectable events becomes much smaller (Marczak et al., 2017). In addition, we found that, the plot of the ratio of the event frequency (EF) of AuNP-P1-NA-P2 to that of AuNP-P1-NA versus the ratio of the EF of AuNP-P1-NA to that of AuNP-P1 could be used to not only determine the number of mutations but also to provide information regarding the mutation site. As shown in Fig. 5b, in general, if the mismatch occurred near the 5′-end of the DNA sequence (i.e., corresponding to the hybridization probe P1), the EF ratio of AuNP-P1-NA-P2 to AuNP-P1-NA was large (1.2–1.8), while that of AuNP-P1-NA to AuNP-P1 had a very small value (0.1–0.2). In contrast, if the mismatch occurred near the 3′-end (corresponding to the hybridization probe P2), the EF ratio of AuNP-P1-NA-P2 to AuNP-P1-NA was small (0.3–0.6, relative to 2.0), while that of AuNP-P1-NA to AuNP-P1 had a large value (0.4–0.7, relative to 0.8). Furthermore, the larger the EF ratio of AuNP-P1-NA-P2 to AuNP-P1-NA and/or the larger

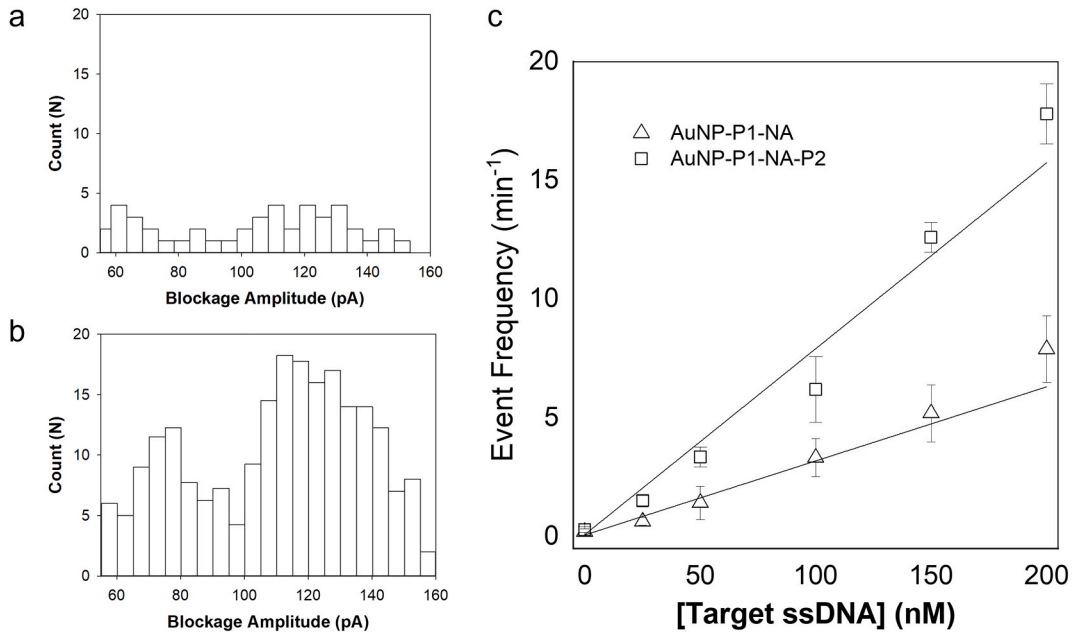

Fig. 4. Nanopore detection of target ssDNA. Representative event amplitude histograms of (a) 25 nM and (b) 100 nM of target DNA; and (c) the plot of event frequency versus target DNA concentration. The experiments were performed at +600 mV in the presence of 1 μM of AuNP-P1 and 2 μM of P2.

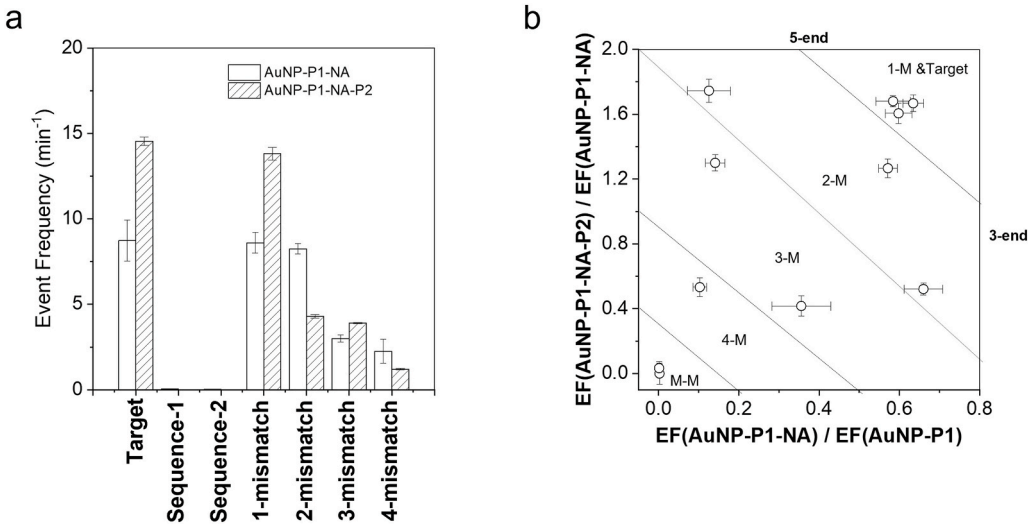

Fig. 5. (a) Selectivity study, and (b) mutation mapping. The experiments were performed at +600 mV in a symmetric buffer condition with both the PET nanopore base and tip compartments filled with 0.5 M KCl and 10 mM Tris (pH 8.0). The concentrations of DNA samples used were 200 nM each. The sequences of DNA samples in Fig. 5 were summarized in Table S1. The one-mismatch, two-mismatch, 3-mismatch, and 4-mismtach results shown in Fig. 5a were based on DNA sample 1-M-2, 2-M-3, 3-M-1, and 4-M, respectively.

the EF ratio of AuNP-P1-NA to AuNP-P1 was, the fewer mutations the DNA sample had.

3.6. *Improving sensor sensitivity via a salt gradient*

Use of an asymmetric electrolyte gradient instead of the conventional symmetric electrolyte solution is a well-established approach to significantly increase the event frequency for the translocation of DNA/RNA molecules through the nanopore (Roozbahani et al., 2017), thus improving the sensor sensitivity for nucleic acid analysis. To examine whether this strategy can be employed to improve the sensitivity for target nucleic acid detection using the large size PET nanopore, translocation of AuNP-P1 hybridization complexes in the nanopore under asymmetric electrolyte conditions was further investigated. Since AuNPs tend to aggregate at high salt concentrations, we kept the concentration of KCl in the PET nanopore base-side compartment constant at 0.5 M, but varying the salt concentration in the tip-side compartment from 0.5 M to 2 M (note that the analytes were added in the base compartment). Our experimental results (Figs. S7a, b, and e) showed that, using a salt gradient instead of a symmetric buffer solution, there was indeed a significant increase in the number of DNA translocation events. Specifically, compared with the symmetric electrolyte solution of 0.5 M KCl (base)/0.5 M KCl (tip), a salt gradient of 0.5 M KCl (base)/2.0 M KCl (tip) resulted in a 7-fold increase in the event frequency. Furthermore, we noticed that, with an increase in the salt concentration of the tip compartment, the open channel current increased dramatically but the event blockage amplitude did not change significantly (Fig. S7c). However, the event residence time decreased with an increase in the salt gradient (Fig. S7d). The dose response curve for the target nucleic acid detection under an asymmetric electrolyte solution of 0.5 M KCl (base)/2.0 M KCl (tip) was shown in Fig. S7f with a detection limit of 0.5 nM.

4. Conclusion

In summary, by taking advantage of two DNA hybridization probes (one of which was immobilized on the surface of AuNPs, while the other was free in solution), detection of short length nucleic acids was successfully achieved using a large size (20 nm tip diameter) PET nanopore. Although only two base mismatch resolution was accomplished in this proof-of-concept investigation, a better sensor resolution and accuracy might be obtained using an appropriately engineered PET nanopore instead of the unmodified PET nanopore used in this work, as demonstrated in our previous study (Zhang et al., 2020a). In particular, alumina surface modification (Wang et al., 2021a) should improve both the LOD and the selectivity. Furthermore, solid-state nanopores fabricated in thin (10–30 nm in length) Si_3N_4 membranes may be used as alternative stochastic sensing elements for nucleic acid detection. It has been well-documented that these short solid-state nanopores could provide a better resolution than the long channel-based PET nanopores (Garaj et al., 2013; Lee et al., 2014). Moreover, it could be visualized that a better nanopore sensor resolution and accuracy might be achieved if more hybridization probes were employed. In addition, although the sensing strategy was demonstrated by analysis of a short DNA sequence, it was in principle applicable to detect various nucleic acids, including microRNAs, viral RNAs, and messenger RNAs, using large size nanopores. It is worth mentioning that the effectiveness of utilizing nanopores to analyze real samples has been reported previously by, e.g., Gu's group who used nucleic acid extraction kits to extract microRNA from clinical samples (Wang et al., 2011), and Wang and co-workers who employed the displacement chemical reaction to selectively extract target nucleic acid from whole blood (Wang et al., 2018a), followed by nanopore analysis. Given the ability of a single PET nanopore to be repeatedly used for ~90 times for effective nucleic acid detection (Supporting Information, Fig. S8), our developed nanopore sensing platform may find useful applications in medical diagnosis.

CRediT authorship contribution statement

Youwen Zhang: Conceptualization, Methodology, Investigation, Formal analysis, Data curation, Writing – original draft. **Xiaohan Chen:** Conceptualization, Investigation. **Ceming Wang:** Investigation. **Hsueh-Chia Chang:** Supervision, Project administration, Funding acquisition, Writing – review & editing. **Xiyun Guan:** Conceptualization, Supervision, Project administration, Funding acquisition, Writing – review & editing.

Declaration of competing interest

The authors declare that they have no known competing financial interests or personal relationships that could have appeared to influence the work reported in this paper.

Acknowledgments

This work was financially supported by the National Institutes of Health (2R15GM110632-02), the NIH Common Fund, through the Office of Strategic Coordination/Office of the NIH Director, 1UG3CA241684-01, and National Science Foundation (1708596).

Appendix A. Supplementary data

Supplementary data to this article can be found online at https://doi.org/10.1016/j.bios.2021.113697.

References

Arima, A., Tsutsui, M., Washio, T., Baba, Y., Kawai, T., 2021. Solid-state nanopore platform integrated with machine learning for digital diagnosis of virus infection. Anal. Chem. 93 (1), 215–227.
Armbruster, D.A., Pry, T., 2008. Limit of blank, limit of detection and limit of quantitation. Clin. Biochem. Rev. 29 (Suppl. 1), S49–S52. Suppl 1.
Bayley, H., 2017. Getting to the bottom of the well. Nat. Nanotechnol. 12 (12), 1116–1117.
Bhatt, N., Huang, P.-J.J., Dave, N., Liu, J., 2011. Dissociation and degradation of thiol-modified DNA on gold nanoparticles in aqueous and organic solvents. Langmuir 27 (10), 6132–6137.
Branton, D., Deamer, D.W., Marziali, A., Bayley, H., Benner, S.A., Butler, T., Di Ventra, M., Garaj, S., Hibbs, A., Huang, X., Jovanovich, S.B., Krstic, P.S., Lindsay, S., Ling, X.S., Mastrangelo, C.H., Meller, A., Oliver, J.S., Pershin, Y.V., Ramsey, J.M., Riehn, R., Soni, G.V., Tabard-Cossa, V., Wanunu, M., Wiggin, M., Schloss, J.A., 2008. The potential and challenges of nanopore sequencing. Nat. Biotechnol. 26 (10), 1146–1153.
Chaibun, T., Puenpa, J., Ngamdee, T., Boonapatcharoen, N., Athamanolap, P., O'Mullane, A.P., Vongpunsawad, S., Poovorawan, Y., Lee, S.Y., Lertanantawong, B., 2021. Rapid electrochemical detection of coronavirus SARS-CoV-2. Nat. Commun. 12 (1), 802.
Chen, K., Zhang, M., Chang, Y.-N., Xia, L., Gu, W., Qin, Y., Li, J., Cui, S., Xing, G., 2016. Utilizing gold nanoparticle probes to visually detect DNA methylation. Nanoscale Res Lett 11 (1), 304.
Chen, X., Roozbahani G, M., Ye, Z., Zhang, Y., Ma, R., Xiang, J., Guan, X., 2018a. Label-free detection of DNA mutations by nanopore analysis. ACS Appl. Mater. Interfaces 10 (14), 11519–11528.
Chen, X., Wang, L., Roozbahani, G.M., Zhang, Y., Xiang, J., Guan, X., 2018b. Nanopore label-free detection of single-nucleotide deletion in Baxα/BaxΔ2. Electrophoresis 39 (19), 2410–2416.
Chen, X., Zhang, Y., Mohammadi Roozbahani, G., Guan, X., 2019. Salt-mediated nanopore detection of ADAM-17. ACS Appl. Mater. 2 (1), 504–509.
Chu, D.K.W., Pan, Y., Cheng, S.M.S., Hui, K.P.Y., Krishnan, P., Liu, Y., Ng, D.Y.M., Wan, C.K.C., Yang, P., Wang, Q., Peiris, M., Poon, L.L.M., 2020. Molecular diagnosis of a novel coronavirus (2019-nCoV) causing an outbreak of pneumonia. Clin. Chem. 66 (4), 549–555.
Demers, L.M., Mirkin, C.A., Mucic, R.C., Reynolds, R.A., Letsinger, R.L., Elghanian, R., Viswanadham, G., 2000. A fluorescence-based method for determining the surface coverage and hybridization efficiency of thiol-capped oligonucleotides bound to gold thin films and nanoparticles. Anal. Chem. 72 (22), 5535–5541.
Dorris, D.R., Nguyen, A., Gieser, L., Lockner, R., Lublinsky, A., Patterson, M., Touma, E., Sendera, T.J., Elghanian, R., Mazumder, A., 2003. Oligodeoxyribonucleotide probe accessibility on a three-dimensional DNA microarray surface and the effect of hybridization time on the accuracy of expression ratios. BMC Biotechnol. 3 (1), 6.
Epanchintseva, A.V., Poletaeva, J.E., Pyshnyi, D.V., Ryabchikova, E.I., Pyshnaya, I.A., 2019. Long-term stability and scale-up of noncovalently bound gold nanoparticle-siRNA suspensions. Beilstein J. Nanotechnol. 10, 2568–2578.
Feng, W., Newbigging, A.M., Le, C., Pang, B., Peng, H., Cao, Y., Wu, J., Abbas, G., Song, J., Wang, D.-B., Cui, M., Tao, J., Tyrrell, D.L., Zhang, X.-E., Zhang, H., Le, X.C., 2020. Molecular diagnosis of COVID-19: challenges and research needs. Anal. Chem. 92 (15), 10196–10209.
Garaj, S., Liu, S., Golovchenko, J.A., Branton, D., 2013. Molecule-hugging graphene nanopores. Proc. Natl. Acad. Sci. Unit. States Am. 110 (30), 12192.
Goto, Y., Yanagi, I., Matsui, K., Yokoi, T., Takeda, K.-i., 2018. Identification of four single-stranded DNA homopolymers with a solid-state nanopore in alkaline CsCl solution. Nanoscale 10 (44), 20844–20850.
Haque, F., Li, J., Wu, H.-C., Liang, X.-J., Guo, P., 2013. Solid-state and biological nanopore for real-time sensing of single chemical and sequencing of DNA. Nano Today 8 (1), 56–74.
Harrell, C.C., Choi, Y., Horne, L.P., Baker, L.A., Siwy, Z.S., Martin, C.R., 2006. Resistive-pulse DNA detection with a conical nanopore sensor. Langmuir 22 (25), 10837–10843.
He, F., Liang, L., Zhou, S., Xie, W., He, S., Wang, Y., Tlili, C., Tong, S., Wang, D., 2018. Label-free sensitive detection of microcystin-LR via aptamer-conjugated gold nanoparticles based on solid-state nanopores. Langmuir 34 (49), 14825–14833.
Jiao, J., Duan, C., Xue, L., Liu, Y., Sun, W., Xiang, Y., 2020. DNA nanoscaffold-based SARS-CoV-2 detection for COVID-19 diagnosis. Biosens. Bioelectron. 167, 112479.
Kim, H., Park, M., Hwang, J., Kim, J.H., Chung, D.-R., Lee, K.-s., Kang, M., 2019. Development of label-free colorimetric assay for MERS-CoV using gold nanoparticles. ACS Sens. 4 (5), 1306–1312.
Kono, N., Arakawa, K., 2019. Nanopore sequencing: review of potential applications in functional genomics. Dev. Growth Differ. 61 (5), 316–326.
Kumar Sharma, R., Agrawal, I., Dai, L., Doyle, P.S., Garaj, S., 2019. Complex DNA knots detected with a nanopore sensor. Nat. Commun. 10 (1), 4473.
Larkin, J., Henley, R., Bell, D.C., Cohen-Karni, T., Rosenstein, J.K., Wanunu, M., 2013. Slow DNA transport through nanopores in hafnium oxide membranes. ACS Nano 7 (11), 10121–10128.
Lee, M.-H., Kumar, A., Park, K.-B., Cho, S.-Y., Kim, H.-M., Lim, M.-C., Kim, Y.-R., Kim, K.-B., 2014. A low-noise solid-state nanopore platform based on a highly insulating substrate. Sci. Rep. 4 (1), 7448.
Li, F., Zhang, H., Dever, B., Li, X.-F., Le, X.C., 2013. Thermal stability of DNA functionalized gold nanoparticles. Bioconjugate Chem. 24 (11), 1790–1797.
Li, Q., Ying, Y.-L., Liu, S.-C., Lin, Y., Long, Y.-T., 2019. Detection of single proteins with a general nanopore sensor. ACS Sens. 4 (5), 1185–1189.

Liang, Y., Xiao, M., Wu, D., Lin, Y., Liu, L., He, J., Zhang, G., Peng, L.-M., Zhang, Z., 2020. Wafer-scale uniform carbon nanotube transistors for ultrasensitive and label-free detection of disease biomarkers. ACS Nano 14 (7), 8866–8874.
Lu, W., Wang, L., Li, J., Zhao, Y., Zhou, Z., Shi, J., Zuo, X., Pan, D., 2015. Quantitative investigation of the poly-adenine DNA dissociation from the surface of gold nanoparticles. Sci. Rep. 5 (1), 10158.
Machinek, R.R.F., Ouldridge, T.E., Haley, N.E.C., Bath, J., Turberfield, A.J., 2014. Programmable energy landscapes for kinetic control of DNA strand displacement. Nat. Commun. 5 (1), 5324.
Marczak, S., Smith, E., Senapati, S., Chang, H.-C., 2017. Selectivity enhancements in gel-based DNA-nanoparticle assays by membrane-induced isotachophoresis: thermodynamics versus kinetics. Electrophoresis 38 (20), 2592–2602.
Mereuta, L., Asandei, A., Dragomir, I.S., Bucataru, I.C., Park, J., Seo, C.H., Park, Y., Luchian, T., 2020. Sequence-specific detection of single-stranded DNA with a gold nanoparticle-protein nanopore approach. Sci. Rep. 10 (1), 11323.
Ohta, S., Glancy, D., Chan, W.C.W., 2016. DNA-controlled dynamic colloidal nanoparticle systems for mediating cellular interaction. Science 351 (6275), 841.
Oukhaled, A., Cressiot, B., Bacri, L., Pastoriza-Gallego, M., Betton, J.-M., Bourhis, E., Jede, R., Gierak, J., Auvray, L., Pelta, J., 2011. Dynamics of completely unfolded and native proteins through solid-state nanopores as a function of electric driving force. ACS Nano 5 (5), 3628–3638.
Parak, W.J., Pellegrino, T., Micheel, C.M., Gerion, D., Williams, S.C., Alivisatos, A.P., 2003. Conformation of oligonucleotides attached to gold nanocrystals probed by gel electrophoresis. Nano Lett. 3 (1), 33–36.
Roman, J., Jarroux, N., Patriarche, G., Français, O., Pelta, J., Le Pioufle, B., Bacri, L., 2017. Functionalized solid-state nanopore integrated in a reusable microfluidic device for a better stability and nanoparticle detection. ACS Appl. Mater. Interfaces 9 (48), 41634–41640.
Roozbahani, G.M., Chen, X., Zhang, Y., Juarez, O., Li, D., Guan, X., 2018. Computation-Assisted nanopore detection of thorium ions. Anal. Chem. 90 (9), 5938–5944.
Roozbahani, G.M., Chen, X., Zhang, Y., Wang, L., Guan, X., 2020. Nanopore detection of metal ions: current status and future directions. Small Methods 4 (10), 2000266.
Roozbahani, G.M., Chen, X., Zhang, Y., Xie, R., Ma, R., Li, D., Li, H., Guan, X., 2017. Peptide-mediated nanopore detection of uranyl ions in aqueous media. ACS Sens. 2 (5), 703–709.
Roozbahani, G.M., Zhang, Y., Chen, X., Soflaee, M.H., Guan, X., 2019. Enzymatic reaction-based nanopore detection of zinc ions. Analyst 144 (24), 7432–7436.
Sensale, S., Wang, C., Chang, H.-C., 2020. Resistive amplitude fingerprints during translocation of linear molecules through charged solid-state nanopores. J. Chem. Phys. 153 (3), 035102.
Steel, A.B., Levicky, R.L., Herne, T.M., Tarlov, M.J., 2000. Immobilization of nucleic acids at solid surfaces: effect of oligonucleotide length on layer assembly. Biophys. J. 79 (2), 975–981.
Talaga, D.S., Li, J., 2009. Single-molecule protein unfolding in solid state nanopores. J. Am. Chem. Soc. 131 (26), 9287–9297.
Tellinghuisen, J., Spiess, A.-N., 2014. Comparing real-time quantitative polymerase chain reaction analysis methods for precision, linearity, and accuracy of estimating amplification efficiency. Anal. Biochem. 449, 76–82.
VanGuilder, H.D., Vrana, K.E., Freeman, W.M., 2008. Twenty-five years of quantitative PCR for gene expression analysis. Biotechniques 44 (5), 619–626.
Vlassiouk, I., Siwy, Z.S., 2007. Nanofluidic diode. Nano Lett. 7 (3), 552–556.
Wang, C., Sensale, S., Pan, Z., Senapati, S., Chang, H.-C., 2021a. Slowing down DNA translocation through solid-state nanopores by edge-field leakage. Nat. Commun. 12 (1), 140.
Wang, L., Chen, X., Zhou, S., Roozbahani, G.M., Zhang, Y., Wang, D., Guan, X., 2018a. Displacement chemistry-based nanopore analysis of nucleic acids in complicated matrices. Chem. Commun. 54 (99), 13977–13980.
Wang, Y., Chen, Q., Deng, T., Liu, Z., 2018b. Self-aligned nanopore formed on a SiO2 pyramidal membrane by a multipulse dielectric breakdown method. J. Phys. Chem. C 122 (21), 11516–11523.
Wang, Y., Zhang, Y., Chen, X., Guan, X., Wang, L., 2021b. Analysis with biological nanopore: on-pore, off-pore strategies and application in biological fluids. Talanta 223, 121684.
Wang, Y., Zheng, D., Tan, Q., Wang, M.X., Gu, L.-Q., 2011. Nanopore-based detection of circulating microRNAs in lung cancer patients. Nat. Nanotechnol. 6 (10), 668–674.
Wu, T., Li, X., Fu, Y., Ding, X., Li, Z., Zhu, G., Fan, J., 2020. A highly sensitive and selective fluorescence biosensor for hepatitis C virus DNA detection based on δ-FeOOH and exonuclease III-assisted signal amplification. Talanta 209, 120550.
Xia, D., Huynh, C., McVey, S., Kobler, A., Stern, L., Yuan, Z., Ling, X.S., 2018. Rapid fabrication of solid-state nanopores with high reproducibility over a large area using a helium ion microscope. Nanoscale 10 (11), 5198–5204.
Zhang, X., Servos, M.R., Liu, J., 2012a. Fast pH-assisted functionalization of silver nanoparticles with monothiolated DNA. Chem. Commun. 48 (81), 10114–10116.
Zhang, X., Servos, M.R., Liu, J., 2012b. Surface science of DNA adsorption onto citrate-capped gold nanoparticles. Langmuir 28 (8), 3896–3902.
Zhang, Y., Chen, X., Wang, C., Roozbahani, G.M., Chang, H.-C., Guan, X., 2020a. Chemically functionalized conical PET nanopore for protein detection at the single-molecule level. Biosens. Bioelectron. 165, 112289.
Zhang, Y., Chen, X., Yuan, S., Wang, L., Guan, X., 2020b. Joint entropy-assisted graphene oxide-based multiplexing biosensing platform for simultaneous detection of multiple proteases. Anal. Chem. 92 (22), 15042–15049.
Zhao, V.X.T., Wong, T.I., Zheng, X.T., Tan, Y.N., Zhou, X., 2020. Colorimetric biosensors for point-of-care virus detections. Mater. Sci. Energy Technol. 3, 237–249.